Deciphering the Interplay Between Inflammatory Factors and Brain Structural Features in Epilepsy

Keywords
Epilepsy, Inflammatory factors, Mendelian randomization, Brain structural features, Unsupervised Deep Learning-derived Imaging Phenotypes

Abstract

Introduction
To evaluate potential causal links among circulating inflammatory factors, deep learning–derived brain structural phenotypes (unimodal deep imaging phenotypes, UDIPs), and epilepsy using Mendelian randomization (MR).

Material and methods
We leveraged genome-wide association study (GWAS) summary statistics for 512 UDIPs derived from whole-brain MRI, 91 circulating inflammatory factors, and epilepsy. Two-sample MR was used to systematically estimate: (i) the effects of inflammatory factors on epilepsy, (ii) the effects of inflammatory factors on UDIPs, and (iii) the effects of UDIPs on epilepsy. We further applied two-step MR to explore whether UDIPs may mediate the effects of inflammatory factors on epilepsy. Robustness was assessed using heterogeneity tests, pleiotropy evaluation, and sensitivity analyses.

Results
Several inflammatory factors showed significant associations with epilepsy risk. Genetically predicted higher levels of CCL23, CXCL11, FGF5, GDNF, and VEGFA were associated with increased epilepsy risk, whereas higher LIFR and OPG were associated with reduced risk. MR analyses also identified multiple T1- and T2-weighted UDIP dimensions associated with epilepsy in opposite directions, indicating heterogeneous structural signatures linked to epilepsy liability (e.g., T1 dimension 76 showed a positive association, while other dimensions were inversely associated). Two-step MR suggested that, for selected pathways, UDIPs may account for part of the association between inflammatory factors and epilepsy, consistent with partial mediation. These findings were broadly consistent across heterogeneity, pleiotropy, and sensitivity analyses.

Conclusions
These findings implicate specific inflammatory factors and MRI-derived structural phenotypes in epilepsy susceptibility and suggest that brain structural features may partly lie on pathways linking inflammation to epilepsy, informing biomarker discovery and therapeutic prioritization.

Deciphering the Interplay Between Inflammatory Factors and Brain Structural Features in Epilepsy

Sheng Fang[1], Xingyu Dong[1], Xin Li[1], Sunfu Zhang[1*]

1. Department of Neurosurgery, The Third People's Hospital of Chengdu, No.82, Qing long street, Qingyang District Chengdu 610031, Sichuan Province, China.

*Correspondence: Sunfu Zhang: zhangsunfucd123@163.com

Abstract

Objective

To evaluate potential causal links among circulating inflammatory factors, deep learning–derived brain structural phenotypes (unimodal deep imaging phenotypes, UDIPs), and epilepsy using Mendelian randomization (MR).

Methods

We leveraged genome-wide association study (GWAS) summary statistics for 512 UDIPs derived from whole-brain MRI, 91 circulating inflammatory factors, and epilepsy. Two-sample MR was used to systematically estimate: (i) the effects of inflammatory factors on epilepsy, (ii) the effects of inflammatory factors on UDIPs, and (iii) the effects of UDIPs on epilepsy. We further applied two-step MR to explore whether UDIPs may mediate the effects of inflammatory factors on epilepsy. Robustness was assessed using heterogeneity tests, pleiotropy evaluation, and sensitivity analyses.

Results

Several inflammatory factors showed significant associations with epilepsy risk. Genetically predicted higher levels of CCL23, CXCL11, FGF5, GDNF, and VEGFA were associated with increased epilepsy risk, whereas higher LIFR and OPG were associated with reduced risk. MR analyses also identified multiple T1- and T2-weighted UDIP dimensions associated with epilepsy in opposite directions, indicating heterogeneous structural signatures linked to epilepsy liability (e.g., T1 dimension 76 showed a positive association, while other dimensions were inversely associated). Two-step MR suggested that, for selected pathways, UDIPs may account for part of the association between inflammatory factors and epilepsy, consistent with partial mediation. These findings were broadly consistent across heterogeneity, pleiotropy, and sensitivity analyses.

Conclusion

These findings implicate specific inflammatory factors and MRI-derived structural phenotypes in epilepsy susceptibility and suggest that brain structural features may partly lie on pathways linking inflammation to epilepsy, informing biomarker

discovery and therapeutic prioritization.

Key words: Epilepsy, Inflammatory factors, Brain structural features, Mendelian randomization, Unsupervised Deep Learning-derived Imaging Phenotypes.

Background

Epilepsy is a prevalent neurological disorder affecting an estimated 50 million people worldwide, with marked geographic and population-level heterogeneity in incidence and prevalence [1,2]. Despite major advances in diagnosis and treatment, a substantial proportion of patients remain refractory to conventional antiseizure medications, leading to persistent morbidity and a considerable healthcare burden [1,3]. Recent progress in neuroimaging and genomics has opened new avenues for earlier detection, deeper mechanistic insight, and the development of personalized therapeutic strategies in epilepsy [4]. In particular, magnetic resonance imaging (MRI) is integral to the clinical evaluation of epilepsy, with strong utility for detecting structural lesions and assisting in seizure-focus localization [4–6]. In parallel, therapeutic development has increasingly moved toward precision medicine, prioritizing targeted approaches tailored to epilepsy subtypes and individual patient characteristics [7].

In recent years, circulating inflammatory factors—often used as peripheral indicators of inflammatory activity—have become a major focus in efforts to clarify epilepsy pathophysiology [8–10]. Accumulating evidence suggests that neuroinflammatory processes contribute to epilepsy onset and progression, and that specific circulating mediators, including C-C motif chemokine ligand 23 (CCL23) and vascular endothelial growth factor A (VEGFA), are associated with epilepsy-related risk and disease features [11–13]. In parallel, the application of deep learning to neuroimaging has created new opportunities to interrogate epilepsy-related brain changes beyond conventional MRI readouts. In particular, unsupervised deep learning methods can derive high-dimensional MRI phenotypes that capture subtle patterns of brain structure and tissue properties, enabling the identification of imaging signatures linked to epilepsy [14,15]. Such imaging-derived features may relate to clinical phenotypes and provide a potential bridge between peripheral inflammatory signals

and brain structural alterations relevant to epilepsy.

Although the individual contributions of circulating inflammatory factors and brain MRI measures to epilepsy have been increasingly described, the interplay between these domains—and their causal relevance to epilepsy risk—remains incompletely understood [16]. Mendelian randomization (MR) leverages germline genetic variants as instrumental variables to strengthen causal inference, thereby reducing bias from confounding and limiting reverse causation. In this study, we therefore applied MR to systematically examine the genetically proxied causal relationships among circulating inflammatory factors, deep learning–derived brain MRI phenotypes, and epilepsy. We further used two-step MR to investigate whether brain imaging phenotypes may partially mediate the effects of inflammatory factors on epilepsy risk. Together, this integrative framework provides additional mechanistic insight into epilepsy pathogenesis and may inform future biomarker development and precision therapeutic strategies.

Methods and Materials

Data Sources

We used genome-wide association study (GWAS) summary statistics for 512 unsupervised deep learning–derived imaging phenotypes (UDIPs) to investigate potential causal relationships among circulating inflammatory factors, brain structure, and epilepsy [17]. UDIPs are high-dimensional MRI-derived traits generated by an unsupervised deep learning framework applied to high-quality whole-brain MRI. These phenotypes summarize multiregional variation in brain structure and demonstrate relatively high SNP-based heritability. Compared with conventional imaging-derived phenotypes that rely on predefined regional parcellations and extensive preprocessing, UDIPs require less complex preprocessing and integrate information across multiple brain regions, enabling a more holistic characterization than single-region analyses.

GWAS summary statistics for 91 circulating inflammatory cytokines were obtained from Zhao et al. (2023), which included 14,824 individuals of European ancestry [18].

Circulating cytokine levels were quantified using the Olink Target Inflammation panel and analyzed in conjunction with genome-wide genotypes.

Summary statistics for epilepsy were sourced from the FinnGen consortium (Release R12), including 15,645 cases and 374,605 controls. The dataset is publicly available at: https://r12.finngen.fi/.

Overall, our MR framework addressed three primary questions: 1. whether genetically predicted UDIP-derived brain MRI phenotypes influence epilepsy risk; 2. whether genetically predicted circulating inflammatory factors influence epilepsy risk; and 3. whether genetically predicted circulating inflammatory factors influence UDIP-derived brain MRI phenotypes.

Instrumental Variable Selection

Single-nucleotide polymorphisms (SNPs) were selected as instrumental variables based on an association threshold of $p < 1\times10^{-5}$ with the exposure. To reduce bias from linkage disequilibrium (LD), we performed LD clumping using a 10,000 kb window and $r^2 = 0.001$, retaining the most significant variant in each LD block. Palindromic SNPs were handled by inferring positive-strand alleles where possible, thereby minimizing unnecessary SNP exclusion and preserving statistical power. For each instrument, we calculated the proportion of exposure variance explained (R^2) and assessed instrument strength using the F-statistic; SNPs with $F < 10$ were excluded to limit weak-instrument bias [19,20].

Statistical Analysis

We used two-sample MR (TSMR) to estimate the causal effects of genetically proxied exposures on epilepsy. The inverse-variance weighted (IVW) approach served as the primary analysis [19]. Under the standard MR assumptions (relevance, independence, and exclusion restriction), IVW provides efficient and consistent causal estimates by meta-analyzing SNP-specific Wald ratios. Because the assumption that all variants are valid instruments may be violated in practice (e.g., due to pleiotropy), we performed complementary analyses using the weighted median (WM) estimator and MR-Egger

regression to improve robustness [21,22].

The WM method yields consistent estimates provided that at least 50% of the total instrument weight derives from valid instruments, and is less sensitive to outlying variants than IVW, particularly when heterogeneity is present. MR-Egger regression relaxes the assumption of no directional pleiotropy by including an intercept term; under the Instrument Strength Independent of Direct Effect (InSIDE) assumption, MR-Egger can provide an unbiased causal estimate even when horizontal pleiotropy exists. However, MR-Egger typically has lower statistical power and wider confidence intervals than IVW.

To assess the robustness of our findings, we conducted a series of sensitivity analyses. Cochran's Q statistic was used to evaluate heterogeneity across SNP-specific estimates [23]. When heterogeneity was detected, we applied an IVW random-effects model to obtain more conservative estimates. Horizontal pleiotropy was examined using the MR-Egger intercept test, where a non-zero intercept suggests directional pleiotropy. We additionally used MR-PRESSO to identify potential outlier variants and to provide outlier-corrected causal estimates [24]. Finally, leave-one-out analyses were performed by iteratively removing each SNP to determine whether any single variant disproportionately influenced the overall result [25].

All analyses were conducted in R (version 4.4.1) using the TwoSampleMR package (version 0.6.8) and the MR-PRESSO package (version 1.0).

Mediation Analysis

We applied a TSMR framework to decompose the total effect of circulating inflammatory cytokines on epilepsy into direct and indirect (mediated) components via UDIPs [26–28]. In this framework, the exposure (cytokine level) influences the mediator (UDIP), which in turn affects the outcome (epilepsy). TSMR assumes no exposure–mediator interaction and relies on the standard MR assumptions for each step.

Specifically, we first estimated the total effect of each circulating inflammatory cytokine on epilepsy using univariable MR (β_1). We then obtained two additional

causal estimates: (i) the effect of the mediator (UDIP) on epilepsy (β_2), and (ii) the effect of the exposure (circulating inflammatory cytokine) on the mediator (α). The indirect (mediated) effect was calculated using the product-of-coefficients approach ($\alpha \times \beta_2$). The proportion mediated was computed as the ratio of the indirect effect to the total effect: $(\alpha \times \beta_2) / \beta_1$.

Ethical Approval and Participant Consent

All data analyzed in this study were obtained from **publicly available** GWAS summary statistics. Each contributing GWAS received approval from the relevant institutional ethics committees, and all participants (or their legal representatives, where applicable) provided written informed consent. Because only de-identified, aggregate-level data were used, no additional ethical approval or participant consent was required for the present analyses.

Results

Genetic Instruments for Exposures

The number of SNPs selected as instrumental variables varied across traits. For the 91 circulating inflammatory cytokines, the number of instruments ranged from 13 to 54 (median 32). For the 512 UDIPs, instrument counts ranged from 13 to 88 (median 35). For epilepsy, 42 SNPs were used as instruments (Supplementary Tables 1 – 3). All retained instruments had F-statistics > 10, indicating adequate instrument strength and reducing concerns about weak-instrument bias.

Genetic Causal Associations Between Circulating Inflammatory Cytokines and Epilepsy

Using the IVW framework to evaluate the causal effects of circulating inflammatory cytokines on epilepsy risk, we identified several cytokines with statistically significant associations. Genetically predicted higher levels of C-C motif chemokine ligand 23 (CCL23), C-X-C motif chemokine ligand 11 (CXCL11), fibroblast growth factor 5 (FGF5), glial cell line-derived neurotrophic factor (GDNF), and vascular

endothelial growth factor A (VEGFA) were associated with an increased risk of epilepsy, whereas higher leukemia inhibitory factor receptor (LIFR) and osteoprotegerin (OPG) were associated with a reduced risk. Among these, VEGFA showed the strongest association with epilepsy (OR 1.079, 95% CI 1.035–1.125, P = 0.0003) (Figure 1; Supplementary Table 4).

In the reverse-direction analysis, IVW results indicated that genetic liability to epilepsy was associated with lower circulating levels of interleukin-10 receptor subunit alpha (IL-10RA), interleukin-20 (IL-20), neurturin (NRTN), and sirtuin-2 (SIRT2), with the largest decrease observed for IL-10RA (OR 0.900, 95% CI 0.836–0.969, P = 0.005) (Figure 2; Supplementary Table 4).

Sensitivity analyses supported the robustness of these findings. MR-Egger intercept and MR-PRESSO analyses provided no evidence of directional horizontal pleiotropy (P > 0.05), and funnel plots showed no obvious asymmetry (Supplementary Table 5; Supplementary Figure 1). After outlier assessment/correction, Cochran's Q tests suggested no significant heterogeneity across SNP-specific estimates (P > 0.05) (Supplementary Table 6). In addition, leave-one-out analyses demonstrated that sequential removal of individual SNPs did not materially alter the overall estimates, indicating that the associations were not driven by any single instrument (Supplementary Figure 2).

Genetic Causal Associations Between UDIPs and Epilepsy

To evaluate the causal effects of UDIP-derived brain MRI phenotypes on epilepsy risk, we performed IVW Mendelian randomization across **512 UDIPs**. In total, **13 UDIPs** showed positive associations with epilepsy risk, including **five T1-weighted UDIPs (dimensions 18, 38, 49, 67, 76) and eight T2-weighted UDIPs (dimensions 15, 35, 41, 42, 49, 72, 99, 105)**. Conversely, 17 UDIPs were inversely associated with epilepsy, including nine **T1-weighted UDIPs (dimensions 7, 14, 16, 46, 50, 56, 104, 120, 125) and eight T2-weighted UDIPs (dimensions 12, 13, 55, 58, 81, 91, 96, 99).** Among all UDIPs, T1 dimension 76 exhibited the strongest association with epilepsy risk (OR 1.001, 95% CI 1.0004–1.0018, P = 0.003) (Figure 3; Supplementary Table

7).

In the reverse-direction analyses (epilepsy → UDIPs), genetic liability to epilepsy was associated with lower levels of several UDIP dimensions from **T1-weighted MRI (dimensions 32, 34, 39) and T2-weighted MRI (dimensions 30, 54, 70, 113, 123). In contrast, epilepsy liability was positively associated with multiple UDIP dimensions across both modalities (dimensions 8, 18, 38, 39, 49, 59, 68, 76, 80, 96, 113, 126, 40) (Figure 4; Supplementary Table 7).**

Notably, we observed bidirectional MR evidence between epilepsy and several T1-weighted UDIP dimensions (dimensions 18, 38, and 49), suggesting potential reciprocal relationships or shared underlying biology for these specific imaging-derived traits.

Sensitivity analyses supported the stability of these findings. MR-Egger and MR-PRESSO tests did not indicate significant directional horizontal pleiotropy ($P > 0.05$) (Supplementary Table 8), and funnel plots showed no obvious asymmetry (Supplementary Figure 3). Cochran's Q statistics suggested no substantial heterogeneity across SNP-specific estimates ($P > 0.05$) (Supplementary Table 9). Finally, leave-one-out analyses did not identify influential single variants that materially altered the overall estimates (Supplementary Figure 4).

Mediation Analysis of Candidate UDIPs

In the TSMR analysis (Figure 5), we identified eight UDIPs that showed evidence of involvement in cytokine–UDIP–epilepsy pathways (Table 1). Genetically predicted CCL23 levels were inversely associated with T1-weighted UDIP dimension 14 ($\beta = -4.263$, 95% CI −6.230 to −2.297) and T2-weighted UDIP dimension 96 ($\beta = -1.956$, 95% CI −3.660 to −0.252). Higher CCL23 levels were associated with increased epilepsy risk (OR 1.076, 95% CI 1.024–1.130), whereas both T1 dimension 14 and T2 dimension 96 were inversely associated with epilepsy (OR 0.998, 95% CI 0.996–0.999; and OR 0.998, 95% CI 0.996–1.000, respectively).

Genetically predicted CXCL11 levels were associated with a decrease in T2-weighted UDIP dimension 13 ($\beta = -2.631$, 95% CI −5.019 to −0.242). Higher CXCL11 levels

were associated with higher epilepsy risk (OR 1.071, 95% CI 1.007–1.138), while T2 dimension 13 was inversely associated with epilepsy (OR 0.998, 95% CI 0.997–1.000).

For osteoprotegerin (OPG), genetically predicted levels were inversely associated with T2-weighted UDIP dimension 96 (β = −2.431, 95% CI −4.714 to −0.149) and positively associated with T1-weighted UDIP dimension 46 (β = 9.250, 95% CI 2.095–16.406). Higher OPG levels were associated with a reduced risk of epilepsy (OR 0.933, 95% CI 0.872–0.997), and T1 dimension 46 was also inversely associated with epilepsy (OR 0.999, 95% CI 0.999–1.000).

Genetically predicted GDNF levels were inversely associated with T2-weighted UDIP dimension 35 (β = −3.357, 95% CI −6.592 to −0.122). Higher GDNF levels were associated with increased epilepsy risk (OR 1.067, 95% CI 1.000–1.139), and T2 dimension 35 was positively associated with epilepsy (OR 1.002, 95% CI 1.000–1.003).

For FGF5, genetically predicted levels were inversely associated with T2-weighted UDIP dimension 15 (β = −1.924, 95% CI −3.717 to −0.131) and positively associated with T1-weighted UDIP dimension 7 (β = 3.770, 95% CI 0.819–6.721). Higher FGF5 levels were associated with higher epilepsy risk (OR 1.041, 95% CI 1.002–1.081). In turn, T2 dimension 15 was positively associated with epilepsy (OR 1.001, 95% CI 1.000–1.003), whereas T1 dimension 7 was inversely associated with epilepsy (OR 0.999, 95% CI 0.998–1.000).

Finally, in the mediation assessment, when the estimated indirect effect ($\alpha \times \beta_2$) was in the opposite direction to the total effect, we did not interpret the UDIP as a supportive mediator in that pathway. Accordingly, T2 dimension 96 was not considered to mediate the association between OPG and epilepsy. Similarly, T2 dimension 35 was not considered a mediator of the GDNF–epilepsy association, and T2 dimension 15 and T1 dimension 7 were not considered mediators of the FGF5–epilepsy association.

Discussion

In this study, we applied Mendelian randomization to delineate the genetic causal

architecture linking circulating inflammatory factors, deep learning–derived brain MRI phenotypes (UDIPs), and epilepsy. We identified significant causal associations between several inflammatory factors and epilepsy, with VEGFA showing the most prominent risk-increasing effect (OR = 1.079, P = 0.0003). In parallel, multiple T1- and T2-weighted UDIP dimensions were associated with epilepsy in both directions, indicating heterogeneous structural signatures underlying epilepsy susceptibility. Among these, T1-weighted UDIP dimension 76 demonstrated the strongest positive association with epilepsy risk (OR = 1.001, P = 0.003). Two-step MR further suggested that, for selected cytokines, part of the association with epilepsy may operate through UDIP-related brain structural features. However, mediation was not consistently supported across all examined pathways, highlighting potential heterogeneity in mechanisms and/or limited power for specific mediator models.

Inflammatory signaling is increasingly recognized as a central component of epilepsy pathophysiology. Accumulating evidence indicates that inflammation is not merely a downstream consequence of seizures, but can also contribute to disease initiation and progression. [29,30] Seizures can trigger broad neuroinflammatory responses that may, in turn, promote epileptogenesis by increasing neuronal excitability, disrupting the BBB, and activating glial cells, thereby establishing a self-reinforcing cycle of inflammation and network hyperexcitability. [31–33] Against this background, clarifying the role of circulating inflammatory factors is important for mechanistic insight, biomarker discovery, and therapeutic prioritization. In our MR analyses, genetically predicted higher levels of CCL23, CXCL11, FGF5, GDNF, and VEGFA were associated with an increased risk of epilepsy, whereas higher LIFR and OPG were associated with a reduced risk, further supporting a contributory role for inflammatory pathways in epilepsy susceptibility.

Several of the identified factors have biologically plausible links to seizure-related brain changes. VEGFA, a key regulator of angiogenesis and vascular remodeling, also participates in neurodevelopment and repair processes. In epilepsy, VEGFA signaling may relate to cerebrovascular remodeling, inflammatory activation, and alterations in neuronal excitability. Notably, elevated VEGFA has been reported to increase BBB

permeability, potentially destabilizing the brain microenvironment and facilitating seizures. [34] In experimental models, Jeong et al. showed that VEGFA can aggravate clinical phenotypes by enhancing vascular permeability and activating glial cells. [35] In addition, chemokines such as CCL23 and CXCL11 are critical for immune-cell recruitment and neuroimmune signaling. [36–38] Prior studies suggest that chemokines contribute to epilepsy through neuroimmune activation and inflammatory amplification at seizure foci. [39,40] Excessive chemokine activity may promote immune-cell accumulation, intensify local inflammation, exacerbate neuronal injury, and increase seizure propensity. [41] Consistent with these observations, our findings support risk-increasing effects of genetically predicted CCL23 and CXCL11 levels, aligning with a model in which heightened chemokine signaling sustains inflammatory microenvironments permissive to seizures. Finally, FGF5 and GDNF are often discussed in the context of neuroprotection and tissue repair. [42,43] GDNF promotes neuronal survival and functional recovery and has been widely studied in epilepsy-related neurobiology. [43,44] Although some experimental work suggests that increasing GDNF may reduce seizure severity—potentially via synaptic plasticity modulation—its effects likely depend on timing, brain region, and cellular context. [45] FGF5 may also influence epilepsy-related processes indirectly through glial proliferation and tissue remodeling after injury. [46] Taken together, these observations highlight that inflammatory and trophic signaling pathways may exert complex, context-dependent effects in epilepsy, underscoring the need for mechanistic and longitudinal studies to clarify when and where these factors are pathogenic versus compensatory.

The interplay between inflammatory signaling and brain structure is also likely to be relevant to epilepsy pathogenesis. Circulating inflammatory mediators may reshape the brain microenvironment—particularly via effects on glial activation and BBB integrity—thereby indirectly influencing seizure susceptibility and disease progression. [47] Chronic inflammatory stimulation can activate microglia and astrocytes and promote a reactive state that enhances network excitability and lowers seizure thresholds. Consistent with this, glial activation and BBB dysfunction have

been implicated as key components of epileptogenesis. [48,49] Moreover, peripheral inflammatory factors may be linked to epilepsy through their associations with MRI-derived brain phenotypes, providing a potential bridge between systemic inflammation and structural brain alterations. [49,50] In our mediation framework, we observed evidence that selected inflammatory factors may influence epilepsy risk through UDIP-defined structural features. For example, genetically predicted CCL23 levels were inversely associated with a T1-weighted UDIP dimension (dimension 14) that was itself inversely associated with epilepsy, suggesting that CCL23-related inflammatory signaling may relate to epilepsy partly through structural phenotypes captured by UDIPs. Similarly, CXCL11 and GDNF showed associations with specific T2-weighted UDIP dimensions, supporting the concept that inflammatory and trophic pathways may converge on brain structural features relevant to epilepsy vulnerability. Taken together, our findings support a model in which inflammatory factors may contribute to epilepsy through both direct and indirect mechanisms, potentially involving neuroimmune activation, BBB perturbation, glial reactivity, and downstream structural brain changes. Factors such as VEGFA, CCL23, CXCL11, FGF5, and GDNF emerge as candidates for further investigation, although their roles may be context dependent and may reflect a mixture of pathogenic and compensatory processes. Future studies should map UDIP dimensions to interpretable neuroanatomical substrates, validate these associations in independent multi-ancestry cohorts, and integrate longitudinal imaging and experimental data to clarify mechanistic pathways and evaluate translational potential for risk stratification and targeted intervention.

Integrating advanced neuroimaging—particularly deep learning–derived MRI phenotypes such as UDIPs—may provide new opportunities for epilepsy risk stratification and the development of personalized management strategies. With continued improvements in MRI acquisition and the rapid maturation of representation-learning approaches, UDIPs have emerged as a promising framework for capturing subtle, distributed patterns of brain structure that may not be apparent using conventional region-based measures. Increasing efforts have therefore focused

on leveraging these high-dimensional imaging signatures to improve early detection, refine phenotypic characterization, and potentially support monitoring of treatment response in epilepsy. Methodologically, UDIPs are designed to learn latent features directly from MRI data, enabling extraction of biologically informative variation that can be difficult to capture with traditional, predefined parcellation-based pipelines. In our analyses, several UDIP dimensions showed evidence of bidirectional MR associations with epilepsy, suggesting a more complex relationship than a purely one-way causal pathway. In particular, T1-weighted UDIP dimensions 18, 38, and 49 demonstrated bidirectional genetic associations with epilepsy, consistent with the possibility that these imaging features may reflect both (i) structural phenotypes that contribute to epilepsy susceptibility and (ii) downstream brain changes associated with epilepsy liability or disease-related processes. This bidirectionality highlights the potential value of such features as risk markers while also emphasizing that some imaging signatures may represent disease-related remodeling rather than solely antecedent causes.

Our analyses also extend prior work by linking circulating inflammatory factors to MRI-derived brain phenotypes, reinforcing the concept that inflammation may contribute to epilepsy through pathways that involve structural brain alterations. Using the TSMR framework, we identified several cytokines—most notably CCL23, CXCL11, and GDNF—that were associated with specific T1- and T2-weighted UDIP dimensions, with corresponding associations between those UDIPs and epilepsy risk. Together, these results provide genetic evidence consistent with the hypothesis that inflammatory signaling may shape brain structural characteristics captured by UDIPs and thereby influence epilepsy susceptibility. At the same time, our mediation results suggest that such imaging features do not uniformly explain cytokine–epilepsy associations across all pathways, underscoring mechanistic heterogeneity and the likelihood of multiple, parallel routes linking inflammation to epilepsy. Nonetheless, the observed cytokine–UDIP–epilepsy relationships are concordant with experimental and clinical observations that inflammatory mediators can remodel the brain microenvironment and contribute to epileptogenesis. Future studies should focus on

mapping UDIP dimensions to interpretable neuroanatomical and microstructural substrates, integrating longitudinal imaging and inflammatory profiling, and testing causal mechanisms in experimental models. Such work would clarify how specific inflammatory pathways translate into structural brain changes and could support the development of precision medicine strategies for epilepsy prevention and treatment.

The principal strengths of this study include the use of Mendelian randomization, which leverages genetic instruments to interrogate potential causal relationships among circulating inflammatory factors, UDIP-derived brain MRI phenotypes, and epilepsy. By design, this framework mitigates confounding and reduces the risk of reverse causation that often limits conventional observational analyses. A further strength is the incorporation of unsupervised deep learning–derived imaging phenotypes (UDIPs), which capture distributed, high-dimensional structural information from MRI and may be more sensitive to subtle brain alterations than traditional region-based measures. In addition, the two-step MR mediation framework enabled us to explore whether brain structural phenotypes may lie on pathways linking inflammatory factors to epilepsy, thereby providing a more integrated view of disease biology. Finally, the use of large-scale GWAS summary statistics improved statistical power and supports the robustness of the genetic associations identified.

Several limitations warrant consideration. First, the underlying GWAS datasets were largely derived from specific ancestral groups (predominantly European), which may limit generalizability and introduce population-specific effects; replication in diverse ancestries is therefore essential. Second, although we performed extensive sensitivity analyses to probe pleiotropy and heterogeneity, MR remains dependent on instrument validity and cannot fully exclude residual violations of MR assumptions. Third, while high-dimensional UDIPs increase sensitivity, they also reduce interpretability, as the biological and neuroanatomical substrates of individual UDIP dimensions are not always straightforward. Finally, we lacked direct multicenter clinical validation and longitudinal phenotyping, which will be important for assessing clinical utility and temporal ordering. Future studies should validate these findings across independent and multi-ancestry cohorts, improve UDIP interpretability through neuroanatomical

mapping, and integrate longitudinal imaging and clinical data to strengthen translational relevance.

Conclusion

This study systematically evaluated the causal links between circulating inflammatory factors, MRI-derived brain structural features (UDIPs), and epilepsy. Our findings support a role for inflammation and structural brain alterations in epilepsy susceptibility, providing a genetic epidemiological framework that may inform earlier risk stratification and offer mechanistic insights. Limitations include potential population bias, model complexity, and the absence of multicenter clinical validation; future work should validate these associations across diverse ancestries and independent cohorts, refine imaging-feature interpretability, and integrate broader clinical and longitudinal datasets to advance precision diagnosis and treatment of epilepsy.

DATA AVAILABILITY

There are restrictions to the availability of data from the FinnGen consortium (R12 release, https://r12.finngen.fi/) and GWAS Catalog (https://www.ebi.ac.uk/).

ACKNOWLEDGEMENTS

We would like to express our sincere gratitude to the public databases that provided the essential data for this study. We acknowledge the valuable contributions of the researchers and organizations that maintain and update these resources. Additionally, we are deeply thankful to the developers of R software and its associated packages, whose tools were crucial in conducting our analysis. Their open-source contributions have significantly advanced the accessibility and capabilities of data analysis in the scientific community. Without these invaluable resources, this research would not have been possible.

AUTHOR CONTRIBUTIONS

SF, XD, XL, and SZ conceptualized the current data analysis; SF and SZ performed statistical

analyses; SF, XD, and XL drafted the manuscript; Overall design collection of data was provided by SF and SZ. All authors have read and agreed to the published version of the manuscript.

FUNDING

No funding.

COMPETING INTERESTS

The authors declare no competing interests.

References

[1] Kanner AM, Bicchi MM. Antiseizure Medications for Adults With Epilepsy: A Review. *JAMA*. 2022 Apr 5;327(13):1269-1281. doi: 10.1001/jama.2022.3880.

[2] Christensen J, Trabjerg BB, Wagner RG, et al. Prevalence of epilepsy: a population-based cohort study in Denmark with comparison to Global Burden of Disease (GBD) prevalence estimates. *J Neurol Neurosurg Psychiatry*. Published online November 27, 2024. doi:10.1136/jnnp-2024-334547.

[3] Lattanzi S, Trinka E, Striano P, et al. Highly Purified Cannabidiol for Epilepsy Treatment: A Systematic Review of Epileptic Conditions Beyond Dravet Syndrome and Lennox-Gastaut Syndrome. *CNS Drugs*. 2021;35(3):265-281. doi:10.1007/s40263-021-00807-y

[4] García-Ramó KB, Sanchez-Catasus CA, Winston GP. Deep learning in neuroimaging of epilepsy. Clin Neurol Neurosurg. 2023;232:107879. doi:10.1016/j.clineuro.2023.107879

[5] Duncan JS, Trimmel K. Advanced neuroimaging techniques in epilepsy. *Curr Opin Neurol*. 2022;35(2):189-195. doi:10.1097/WCO.0000000000001007

[6] Lucas A, Revell A, Davis KA. Artificial intelligence in epilepsy - applications and pathways to the clinic. *Nat Rev Neurol*. 2024;20(6):319-336. doi:10.1038/s41582-024-00965-9

[7] Löscher W, Potschka H, Sisodiya SM, Vezzani A. Drug Resistance in Epilepsy:

Clinical Impact, Potential Mechanisms, and New Innovative Treatment Options. *Pharmacol Rev*. 2020;72(3):606-638. doi:10.1124/pr.120.019539

[8] Marta B, Białecka M, Machoy-Mokrzyńska A, Malinowski D, Rać M. The Importance of TNF-α Signaling – Potential Risk Factor in Neurodegenerative and Cardiovascular Diseases. *Archives of Medical Science*. 2025. doi:10.5114/aoms/201446.

[9] Zhang L, Li J, Zhang Y, Zhang H. Sanguiin inhibits cerebral hemorrhage in rats by protecting the blood-brain barrier. *Archives of Medical Science*. 2024;20(4):1345–1348. doi:10.5114/aoms/193019.

[10] Zabrodskaya Y, Paramonova N, Litovchenko A, et al. Neuroinflammatory Dysfunction of the Blood-Brain Barrier and Basement Membrane Dysplasia Play a Role in the Development of Drug-Resistant Epilepsy. *Int J Mol Sci*. 2023;24(16):12689. doi:10.3390/ijms241612689

[11] Zhu X, Liu J, Chen O, et al. Neuroprotective and anti-inflammatory effects of isoliquiritigenin in kainic acid-induced epileptic rats via the TLR4/MYD88 signaling pathway. *Inflammopharmacology*. 2019 Dec;27(6):1143-1153. doi: 10.1007/s10787-019-00592-7.

[12] Lange C, Storkebaum E, de Almodóvar CR, Dewerchin M, Carmeliet P. Vascular endothelial growth factor: a neurovascular target in neurological diseases. *Nat Rev Neurol*. 2016 Aug;12(8):439-54. doi: 10.1038/nrneurol.2016.88.

[13] Guo D, Zhang B, Han L, Rensing NR, Wong M. Cerebral vascular and blood brain-barrier abnormalities in a mouse model of epilepsy and tuberous sclerosis complex. *Epilepsia*. 2024 Feb;65(2):483-496. doi: 10.1111/epi.17848.

[14] Rüber T, David B, Elger CE. MRI in epilepsy: clinical standard and evolution. *Curr Opin Neurol*. 2018 Apr;31(2):223-231. doi: 10.1097/WCO.0000000000000539.

[15] Xiao F, Caciagli L, Wandschneider B, et al. Identification of different MRI atrophy progression trajectories in epilepsy by subtype and stage inference. *Brain*. 2023;146(11):4702-4716. doi:10.1093/brain/awad284.

[16] Chen J, Ragab AAY, Doyle MF, et al. Inflammatory protein associations with brain MRI measures: Framingham Offspring Cohort. *Alzheimers Dement*.

2024;20(11):7465-7478. doi:10.1002/alz.14147.

[17] Patel K, Xie Z, Yuan H, et al. Unsupervised deep representation learning enables phenotype discovery for genetic association studies of brain imaging. *Commun Biol*. 2024;7(1):414. doi:10.1038/s42003-024-06096-7.

[18] Zhao JH, Stacey D, Eriksson N, et al. Genetics of circulating inflammatory proteins identifies drivers of immune-mediated disease risk and therapeutic targets. *Nat Immunol*. 2023;24(9):1540-1551. doi:10.1038/s41590-023-01588-w.

[19] Palmer TM, Lawlor DA, Harbord RM, et al. Using multiple genetic variants as instrumental variables for modifiable risk factors. *Stat Methods Med Res*. 2012;21(3):223-242. doi:10.1177/0962280210394459.

[20] Lawlor DA, Harbord RM, Sterne JA, Timpson N, Davey Smith G. Mendelian randomization: using genes as instruments for making causal inferences in epidemiology. *Stat Med*. 2008;27(8):1133-1163. doi:10.1002/sim.3034.

[21] Bowden J, Davey Smith G, Haycock PC, Burgess S. Consistent Estimation in Mendelian Randomization with Some Invalid Instruments Using a Weighted Median Estimator. *Genet Epidemiol*. 2016;40(4):304-314. doi:10.1002/gepi.21965.

[22] Bowden J, Davey Smith G, Burgess S. Mendelian randomization with invalid instruments: effect estimation and bias detection through Egger regression. *Int J Epidemiol*. 2015;44(2):512-525. doi:10.1093/ije/dyv080.

[23] Egger M, Smith GD, Phillips AN. Meta-analysis: principles and procedures. *BMJ*. 1997;315(7121):1533-1537. doi:10.1136/bmj.315.7121.1533

[24] Verbanck M, Chen CY, Neale B, Do R. Publisher Correction: Detection of widespread horizontal pleiotropy in causal relationships inferred from Mendelian randomization between complex traits and diseases. *Nat Genet*. 2018;50(8):1196. doi:10.1038/s41588-018-0164-2

[25] Austin GI, Pe'er I, Korem T. Distributional bias compromises leave-one-out cross-validation. *Sci Adv.* 2025;11(48):eadx6976. doi:10.1126/sciadv.adx6976.

[26] Yuan J, Xiong X, Zhang B, et al. Genetically predicted C-reactive protein mediates the association between rheumatoid arthritis and atlantoaxial subluxation. *Front Endocrinol (Lausanne).* 2022;13:1054206.

doi:10.3389/fendo.2022.1054206

[27] Li Z, Wei H, Tang X, Liu T, Li S, Wang X. Blood metabolites mediate the impact of lifestyle factors on the risk of urolithiasis: a multivariate, mediation Mendelian randomization study. *Urolithiasis*. 2024;52(1):44. doi:10.1007/s00240-024-01545-8

[28] Li F, Zhao Q, Tang T, et al. Brain imaging derived phenotypes: a biomarker for the onset of inflammatory bowel disease and a potential mediator of mental complications. *Front Immunol*. 2024;15:1359540. doi:10.3389/fimmu.2024.1359540

[29] Dong X, Fan J, Lin D, et al. Captopril alleviates epilepsy and cognitive impairment by attenuation of C3-mediated inflammation and synaptic phagocytosis. *J Neuroinflammation*. 2022;19(1):226. doi:10.1186/s12974-022-02587-8.

[30] Terrone G, Balosso S, Pauletti A, Ravizza T, Vezzani A. Inflammation and reactive oxygen species as disease modifiers in epilepsy. *Neuropharmacology*. 2020;167:107742. doi:10.1016/j.neuropharm.2019.107742

[31] Purnell BS, Alves M, Boison D. Astrocyte-neuron circuits in epilepsy. *Neurobiol Dis*. 2023;179:106058. doi:10.1016/j.nbd.2023.106058

[32] Meng S, Cao H, Huang Y, et al. ASK1-K716R reduces neuroinflammation and white matter injury via preserving blood-brain barrier integrity after traumatic brain injury. *J Neuroinflammation*. 2023;20(1):244. doi:10.1186/s12974-023-02923-6

[33] Liu C, Zhao XM, Wang Q, et al. Astrocyte-derived SerpinA3N promotes neuroinflammation and epileptic seizures by activating the NF-κB signaling pathway in mice with temporal lobe epilepsy. *J Neuroinflammation*. 2023;20(1):161. doi:10.1186/s12974-023-02840-8

[34] Castañeda-Cabral JL, Colunga-Durán A, Ureña-Guerrero ME, et al. Expression of VEGF- and tight junction-related proteins in the neocortical microvasculature of patients with drug-resistant temporal lobe epilepsy. *Microvasc Res*. 2020;132:104059. doi:10.1016/j.mvr.2020.104059

[35] Jeong KH, Cho KO, Lee MY, Kim SY, Kim WJ. Vascular endothelial growth factor receptor-3 regulates astroglial glutamate transporter-1 expression via mTOR activation in reactive astrocytes following pilocarpine-induced status epilepticus. *Glia*. 2021;69(2):296-309. doi:10.1002/glia.23897

[36] Du X, Li F, Zhang C, et al. Eosinophil-derived chemokine (hCCL15/23, mCCL6) interacts with CCR1 to promote eosinophilic airway inflammation. *Signal Transduct Target Ther*. 2021;6(1):91. doi:10.1038/s41392-021-00482-x

[37] Li Y, Han S, Wu B, et al. CXCL11 Correlates with Immune Infiltration and Impacts Patient Immunotherapy Efficacy: A Pan-Cancer Analysis. *Front Immunol*. 2022;13:951247. doi:10.3389/fimmu.2022.951247

[38] Zhao Y, Li T, Jiang Z, et al. The miR-9-5p/CXCL11 pathway is a key target of hydrogen sulfide-mediated inhibition of neuroinflammation in hypoxic ischemic brain injury. *Neural Regen Res*. 2024;19(5):1084-1094. doi:10.4103/1673-5374.382860

[39] Gupta S, Viotti A, Eichwald T, et al. Navigating the blurred path of mixed neuroimmune signaling. *J Allergy Clin Immunol*. 2024;153(4):924-938. doi:10.1016/j.jaci.2024.02.006

[40] Cerri C, Caleo M, Bozzi Y. Chemokines as new inflammatory players in the pathogenesis of epilepsy. *Epilepsy Res*. 2017;136:77-83. doi:10.1016/j.eplepsyres.2017.07.016

[41] Wu Q, Wang H, Liu X, Zhao Y, Su P. Microglial activation and over pruning involved in developmental epilepsy. *J Neuropathol Exp Neurol*. 2023;82(2):150-159. doi:10.1093/jnen/nlac111

[42] Parthasarathy G, Pattison MB, Midkiff CC. The FGF/FGFR system in the microglial neuroinflammation with Borrelia burgdorferi: likely intersectionality with other neurological conditions. *J Neuroinflammation*. 2023;20(1):10. doi:10.1186/s12974-022-02681-x

[43] Fei J, Chen S, Song X, et al. Exogenous GDNF promotes peripheral facial nerve regeneration in rats through the PI3K/AKT/mTOR signaling pathway. *FASEB J*. 2024;38(1):e23340. doi:10.1096/fj.202301664R

[44] Eggers R, de Winter F, Tannemaat MR, Malessy MJA, Verhaagen J. GDNF Gene Therapy to Repair the Injured Peripheral Nerve. *Front Bioeng Biotechnol*. 2020;8:583184. doi:10.3389/fbioe.2020.583184

[45] Shpak AA, Rider FK, Druzhkova TA, et al. Reduced Levels of Lacrimal Glial Cell Line-Derived Neurotrophic Factor (GDNF) in Patients with Focal Epilepsy and

Focal Epilepsy with Comorbid Depression: A Biomarker Candidate. *Int J Mol Sci*. 2023;24(23):16818. doi:10.3390/ijms242316818

[46] Parthasarathy G, Pattison MB, Midkiff CC. The FGF/FGFR system in the microglial neuroinflammation with Borrelia burgdorferi: likely intersectionality with other neurological conditions. *J Neuroinflammation*. 2023;20(1):10. doi:10.1186/s12974-022-02681-x

[47] Liu L, Wang W, Huang L, et al. Injectable pathological microenvironment-responsive anti-inflammatory hydrogels for ameliorating intervertebral disc degeneration. *Biomaterials*. 2024;306:122509. doi:10.1016/j.biomaterials.2024.122509

[48] An W, Xing M, Fan W, Zheng K, Xu X. The ketogenic diet alleviates neuronal ferroptosis in epilepsy via HDAC4/TFRC signalling. *Archives of Medical Science*. 2025. doi:10.5114/aoms/207708.

[49] Alyu F, Dikmen M. Inflammatory aspects of epileptogenesis: contribution of molecular inflammatory mechanisms. *Acta Neuropsychiatr*. 2017;29(1):1-16. doi:10.1017/neu.2016.47

[50] Hayek D, Ziegler G, Kleineidam L, et al. Different inflammatory signatures based on CSF biomarkers relate to preserved or diminished brain structure and cognition. *Mol Psychiatry*. 2024;29(4):992-1004. doi:10.1038/s41380-023-02387-3

Figure legends

Figure 1. Forest plot to visualize the causal effects of circulating inflammatory cytokines and epilepsy.

Figure 2. Forest plot to visualize the causal effects of epilepsy and circulating inflammatory cytokines.

Figure 3. Forest plot to visualize the causal effects of Unsupervised Deep learning derived Imaging Phenotypes and epilepsy.

Figure 4. Forest plot to visualize the causal effects of epilepsy and Unsupervised Deep learning derived Imaging Phenotypes.

Figure 5. Forest plot to visualize the causal effects of circulating inflammatory cytokines and Unsupervised Deep learning derived Imaging Phenotypes.

Supplementary Figure 1. Mendelian randomization (MR) scatter plots for the associations between genetically predicted circulating inflammatory factors and epilepsy. The x-axis shows the SNP–exposure association (effect estimate for each genetic instrument on the inflammatory factor), and the y-axis shows the SNP–outcome association (effect estimate on epilepsy, on the log-odds scale). Each point represents an instrumental SNP. The fitted lines indicate MR causal estimates using the inverse-variance weighted (IVW) and MR-Egger methods. Panels show MR results for (A) CCL23, (B) CXCL11, (C) FGF5, (D) GDNF, (E) LIFR, (F) OPG, and (G) VEGFA in relation to epilepsy.

Supplementary Figure 2. Mendelian randomization (MR) scatter plots for the associations between genetic liability to epilepsy and circulating inflammatory factors. The x-axis shows the SNP–exposure association (effect estimate of each instrumental SNP on epilepsy, on the log-odds scale), and the y-axis shows the SNP–outcome association (effect estimate on the circulating protein level). Each point represents an instrumental SNP. The fitted lines denote MR causal estimates derived from the inverse-variance weighted (IVW) and MR-Egger methods. Panels show MR results for epilepsy in relation to (A) IL-10RA, (B) IL-20, (C) NRTN, and (D) SIRT2.

Supplementary Figure 3. Leave-one-out sensitivity analyses for the Mendelian randomization (MR) estimates of circulating inflammatory factors on epilepsy. Each panel shows the IVW MR estimate recalculated after sequentially excluding one instrumental SNP at a time. Points indicate the leave-one-out causal estimate, and horizontal lines represent the corresponding 95% confidence intervals. Consistency of

the estimates across exclusions suggests that the overall MR results are not driven by any single SNP. Panels correspond to (A) CCL23, (B) CXCL11, (C) FGF5, (D) GDNF, (E) LIFR, (F) OPG, and (G) VEGFA in relation to epilepsy.

Supplementary Figure 4. Leave-one-out sensitivity analyses for the Mendelian randomization (MR) estimates of genetic liability to epilepsy on circulating inflammatory factors. Each panel shows the IVW MR estimate recalculated after iteratively removing one instrumental SNP at a time. Points represent the leave-one-out causal estimates, and horizontal bars indicate 95% confidence intervals. Stable estimates across exclusions suggest that the overall results are not driven by a single SNP. Panels correspond to epilepsy in relation to (A) IL-10RA, (B) IL-20, (C) NRTN, and (D) SIRT2.

Supplementary Figure 5. Mendelian randomization (MR) scatter plots for the associations between T1-weighted UDIP dimensions and epilepsy. The x-axis shows the SNP–exposure association (effect estimate of each instrumental SNP on the UDIP dimension), and the y-axis shows the SNP–outcome association (effect estimate on epilepsy, on the log-odds scale). Each point represents an instrumental SNP. The fitted lines indicate MR causal estimates using the inverse-variance weighted (IVW) and MR-Egger methods. Panels correspond to T1-weighted UDIP dimensions: (A) 7, (B) 14, (C) 18, (D) 46, (E) 49, (F) 56, (G) 104, (H) 120, (I) 16, (J) 38, (K) 50, (L) 67, (M) 76, and (N) 125.

Supplementary Figure 6. Mendelian randomization (MR) scatter plots for the associations between T2-weighted UDIP dimensions and epilepsy. The x-axis shows the SNP–exposure association (effect estimate of each instrumental SNP on the UDIP dimension), and the y-axis shows the SNP–outcome association (effect estimate on epilepsy, on the log-odds scale). Each point represents an instrumental SNP. The fitted lines indicate MR causal estimates using the inverse-variance weighted (IVW) and MR-Egger methods. Panels correspond to T2-weighted UDIP dimensions: (A) 13, (B)

15, (C) 49, (D) 55, (E) 72, (F) 91, (G) 96, (H) 99, (I) 12, (J) 35, (K) 41, (L) 42, (M) 58, (N) 81, and (O) 105.

Supplementary Figure 7. Leave-one-out sensitivity analyses for the Mendelian randomization (MR) estimates of T1-weighted UDIP dimensions on epilepsy. For each panel, the IVW MR estimate was recalculated after sequentially removing one instrumental SNP at a time. Points represent the leave-one-out causal estimates and horizontal lines denote the corresponding 95% confidence intervals. Consistent estimates across exclusions indicate that the overall MR results are not driven by any single SNP. Panels correspond to T1-weighted UDIP dimensions: (A) 7, (B) 14, (C) 18, (D) 46, (E) 49, (F) 56, (G) 104, (H) 120, (I) 16, (J) 38, (K) 50, (L) 67, (M) 76, and (N) 125.

Supplementary Figure 8. Leave-one-out sensitivity analyses for the Mendelian randomization (MR) estimates of T2-weighted UDIP dimensions on epilepsy. In each panel, the IVW MR estimate was recalculated after iteratively excluding one instrumental SNP at a time. Points represent the leave-one-out causal estimates and horizontal lines indicate the corresponding 95% confidence intervals. Consistency of the estimates across exclusions suggests that the overall MR results are not driven by any single SNP. Panels correspond to T2-weighted UDIP dimensions: (A) 13, (B) 15, (C) 49, (D) 55, (E) 72, (F) 91, (G) 96, (H) 99, (I) 12, (J) 35, (K) 41, (L) 42, (M) 58, (N) 81, and (O) 105.

Supplementary Figure 9. Mendelian randomization (MR) scatter plots for the associations between genetically predicted circulating inflammatory factors and selected UDIP dimensions identified in the mediation analysis. The x-axis shows the SNP–exposure association (effect estimate of each instrumental SNP on the inflammatory factor), and the y-axis shows the SNP–outcome association (effect estimate on the UDIP dimension). Each point represents an instrumental SNP. The fitted lines indicate MR causal estimates derived from the inverse-variance weighted

(IVW) and MR-Egger methods. Panels show MR results for the effect of (A) CCL23 on T1-weighted UDIP dimension 14, (B) CCL23 on T2-weighted UDIP dimension 96, (C) CXCL11 on T2-weighted UDIP dimension 13, (D) FGF5 on T1-weighted UDIP dimension 7, (E) FGF5 on T2-weighted UDIP dimension 15, (F) GDNF on T2-weighted UDIP dimension 35, (G) OPG on T1-weighted UDIP dimension 46, and (H) OPG on T2-weighted UDIP dimension 96.

Supplementary Figure 10. Leave-one-out sensitivity analyses for the Mendelian randomization (MR) estimates of circulating inflammatory factors on selected UDIP dimensions included in the mediation analysis. In each panel, the IVW MR estimate was recalculated after sequentially excluding one instrumental SNP at a time. Points represent the leave-one-out causal estimates and horizontal lines indicate the corresponding 95% confidence intervals. Stable estimates across exclusions suggest that the overall MR results are not driven by any single SNP. Panels show MR results for the effect of (A) CCL23 on T1-weighted UDIP dimension 14, (B) CCL23 on T2-weighted UDIP dimension 96, (C) CXCL11 on T2-weighted UDIP dimension 13, (D) FGF5 on T1-weighted UDIP dimension 7, (E) FGF5 on T2-weighted UDIP dimension 15, (F) GDNF on T2-weighted UDIP dimension 35, (G) OPG on T1-weighted UDIP dimension 46, and (H) OPG on T2-weighted UDIP dimension 96.

Table 1. Two-step Mendelian randomization analyses of the causal effects between circulating inflammatory cytokines, Unsupervised Deep learning derived Imaging Phenotypes and epilepsy, and epilepsy.

Expose	Outcome	method	nsnp	b	se	pval	lo_ci	up_ci	mediated (%)
C-C motif chemokine 23 levels	T1 brain MRIs Unsupervised Deep learning derived Imaging Phenotypes (dimension 14)	Inverse variance weighted	31	-4.264	1.003	2.145×10^{-05}	-6.23	-2.30	12.30
C-C motif chemokine 23 levels	T2 brain MRIs Unsupervised Deep learning derived Imaging Phenotypes (dimension 96)	Inverse variance weighted	31	-1.956	0.869	0.024	-3.66	-0.25	5.59
C-X-C motif chemokine 11 levels	T2 brain MRIs Unsupervised Deep learning derived Imaging Phenotypes (dimension 13)	Inverse variance weighted	38	-2.631	1.219	0.031	-5.02	-0.24	5.79
Osteoprotegerin levels	T1 brain MRIs Unsupervised Deep learning derived Imaging Phenotypes (dimension 46)	Inverse variance weighted	30	9.250	3.651	0.011	2.10	16.41	8.81

Causal links among inflammation, deep learning-derived brain structure and epilepsy: A Mendelian randomization study

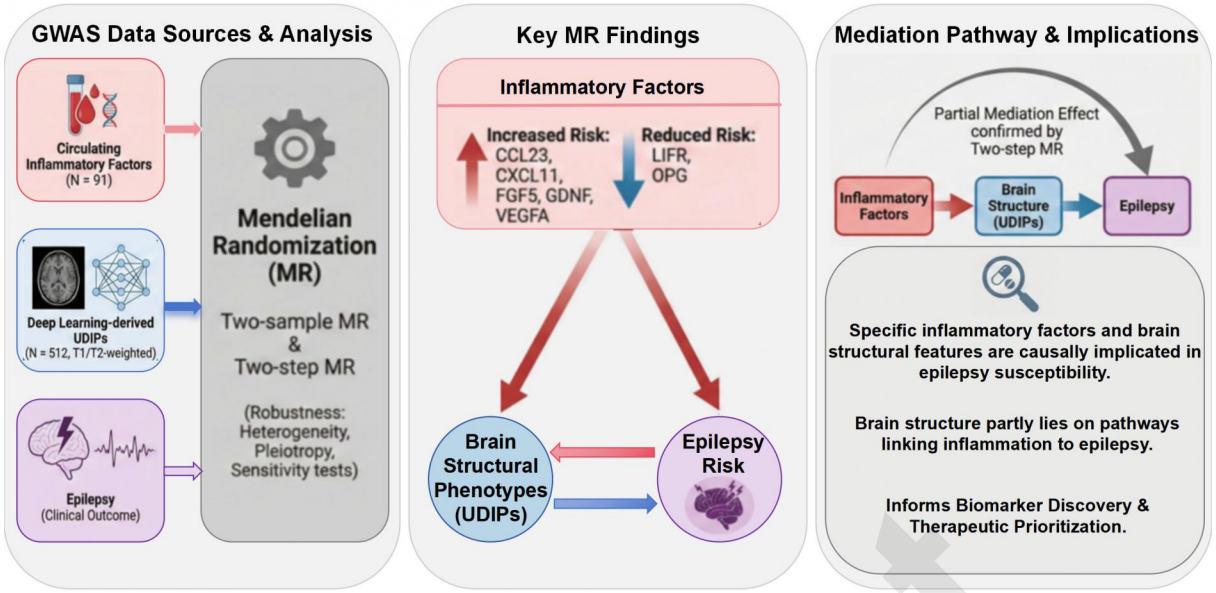

Table 1. Two-step Mendelian randomization

Expose

C-C motif chemokine 23 levels

C-C motif chemokine 23 levels

C-X-C motif chemokine 11 levels

Osteoprotegerin levels

analyses of the causal effects between circulating inflammatory cytokines, Unsupervised Deep learning deriv
Outcome
T1 brain MRIs Unsupervised Deep learning derived Imaging Phenotypes (dimension 14)
T2 brain MRIs Unsupervised Deep learning derived Imaging Phenotypes (dimension 96)
T2 brain MRIs Unsupervised Deep learning derived Imaging Phenotypes (dimension 13)
T1 brain MRIs Unsupervised Deep learning derived Imaging Phenotypes (dimension 46)

ved Imaging Phenotypes and epilepsy, and epilepsy.

method	nsnp	b	se	pval	lo_ci
Inverse vari	31	-4,263590989	1,003366982	2,14E-05	-6,230190273
Inverse vari	31	-1,95599211	0,869239916	0,024434176	-3,659702346
Inverse vari	38	-2,630844792	1,218584536	0,030855211	-5,019270483
Inverse vari	30	9,250451153	3,650733292	0,011281343	2,095013901

up_ci	mediated (%)
-2,296991705	12, 29719156
-0,252281875	5, 592000599
-0,242419101	5, 785621296
16,40588841	8, 810293628

Exposure	method	nsnp	HR (95% CI)	pval
C−C motif chemokine 23 levels	Inverse variance weighted	30	1.08 (1.02 to 1.13)	0.0039
C−X−C motif chemokine 11 levels	Inverse variance weighted	38	1.07 (1.01 to 1.14)	0.0279
Fibroblast growth factor 5 levels	Inverse variance weighted	32	1.04 (1.00 to 1.08)	0.0378
Glial cell line−derived neurotrophic factor levels	Inverse variance weighted	24	1.07 (1.00 to 1.14)	0.0494
Leukemia inhibitory factor receptor levels	Inverse variance weighted	27	0.92 (0.87 to 0.98)	0.0145
Osteoprotegerin levels	Inverse variance weighted	27	0.93 (0.87 to 1.00)	0.0403
Vascular endothelial growth factor A levels	Inverse variance weighted	33	1.08 (1.04 to 1.13)	0.0003

Outcome	method	nsnp	HR (95% CI)	pval
Interleukin−10 receptor subunit alpha levels	Inverse variance weighted	40	0.90 (0.84 to 0.97)	0.0051
Interleukin−20 levels	Inverse variance weighted	40	0.93 (0.87 to 1.00)	0.0356
Neurturin levels	Inverse variance weighted	40	0.92 (0.86 to 0.99)	0.0231
SIR2−like protein 2 levels	Inverse variance weighted	39	0.94 (0.88 to 1.00)	0.0489

Exposure	method	nsnp	HR (95% CI)	pval
T1 brain MRIs UDIPs (dimension 7)	Inverse variance weighted	55	0.9989 (0.9981 to 0.9998)	0.0133
T1 brain MRIs UDIPs (dimension 14)	Inverse variance weighted	54	0.9979 (0.9963 to 0.9995)	0.0097
T1 brain MRIs UDIPs (dimension 18)	Inverse variance weighted	48	1.0016 (1.0003 to 1.0029)	0.0160
T1 brain MRIs UDIPs (dimension 46)	Inverse variance weighted	54	0.9993 (0.9987 to 1.0000)	0.0483
T1 brain MRIs UDIPs (dimension 49)	Inverse variance weighted	45	1.0014 (1.0001 to 1.0027)	0.0330
T1 brain MRIs UDIPs (dimension 56)	Inverse variance weighted	41	0.9989 (0.9979 to 0.9999)	0.0309
T1 brain MRIs UDIPs (dimension 104)	Inverse variance weighted	40	0.9986 (0.9974 to 0.9997)	0.0139
T1 brain MRIs UDIPs (dimension 120)	Inverse variance weighted	60	0.9991 (0.9982 to 1.0000)	0.0403
T1 brain MRIs UDIPs (dimension 7)	Inverse variance weighted	30	0.9993 (0.9987 to 1.0000)	0.0409
T1 brain MRIs UDIPs (dimension 16)	Inverse variance weighted	25	0.9990 (0.9981 to 0.9999)	0.0332
T1 brain MRIs UDIPs (dimension 38)	Inverse variance weighted	29	1.0016 (1.0002 to 1.0031)	0.0288
T1 brain MRIs UDIPs (dimension 50)	Inverse variance weighted	29	0.9993 (0.9985 to 1.0000)	0.0391
T1 brain MRIs UDIPs (dimension 67)	Inverse variance weighted	29	1.0016 (1.0002 to 1.0030)	0.0286
T1 brain MRIs UDIPs (dimension 76)	Inverse variance weighted	26	1.0011 (1.0004 to 1.0018)	0.0034
T1 brain MRIs UDIPs (dimension 125)	Inverse variance weighted	29	0.9989 (0.9979 to 0.9999)	0.0389
T2 brain MRIs UDIPs (dimension 13)	Inverse variance weighted	53	0.9985 (0.9972 to 0.9998)	0.0274
T2 brain MRIs UDIPs (dimension 15)	Inverse variance weighted	38	1.0017 (1.0001 to 1.0032)	0.0343
T2 brain MRIs UDIPs (dimension 49)	Inverse variance weighted	41	1.0022 (1.0003 to 1.0042)	0.0233
T2 brain MRIs UDIPs (dimension 55)	Inverse variance weighted	37	0.9978 (0.9961 to 0.9996)	0.0145
T2 brain MRIs UDIPs (dimension 72)	Inverse variance weighted	52	1.0011 (1.0000 to 1.0022)	0.0473
T2 brain MRIs UDIPs (dimension 91)	Inverse variance weighted	48	0.9979 (0.9961 to 0.9997)	0.0222
T2 brain MRIs UDIPs (dimension 96)	Inverse variance weighted	41	0.9979 (0.9960 to 0.9999)	0.0364
T2 brain MRIs UDIPs (dimension 99)	Inverse variance weighted	36	1.0023 (1.0001 to 1.0045)	0.0430
T2 brain MRIs UDIPs (dimension 12)	Inverse variance weighted	31	0.9988 (0.9976 to 0.9999)	0.0402
T2 brain MRIs UDIPs (dimension 35)	Inverse variance weighted	31	1.0017 (1.0001 to 1.0033)	0.0344
T2 brain MRIs UDIPs (dimension 41)	Inverse variance weighted	24	1.0022 (1.0002 to 1.0043)	0.0351
T2 brain MRIs UDIPs (dimension 42)	Inverse variance weighted	33	1.0011 (1.0001 to 1.0022)	0.0319
T2 brain MRIs UDIPs (dimension 49)	Inverse variance weighted	25	1.0015 (1.0002 to 1.0028)	0.0268
T2 brain MRIs UDIPs (dimension 58)	Inverse variance weighted	26	0.9981 (0.9963 to 1.0000)	0.0480
T2 brain MRIs UDIPs (dimension 81)	Inverse variance weighted	31	0.9986 (0.9974 to 0.9998)	0.0208
T2 brain MRIs UDIPs (dimension 99)	Inverse variance weighted	21	0.9977 (0.9957 to 0.9997)	0.0228
T2 brain MRIs UDIPs (dimension 105)	Inverse variance weighted	20	1.0017 (1.0001 to 1.0032)	0.0319

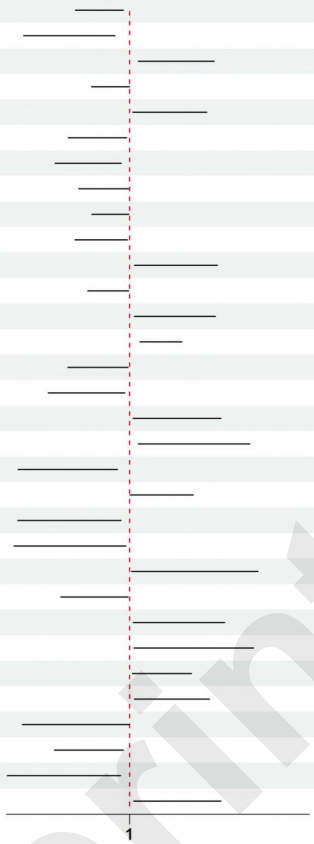

Outcome	method	nsnp	HR (95% CI)	pval
T1 brain MRIs UDIPs (dimension 8)	Inverse variance weighted	36	276.25 (2.24 to 34125.35)	0.0222
T1 brain MRIs UDIPs (dimension 18)	Inverse variance weighted	36	19.18 (1.47 to 249.98)	0.0241
T1 brain MRIs UDIPs (dimension 32)	Inverse variance weighted	36	0.02 (0.00 to 0.62)	0.0248
T1 brain MRIs UDIPs (dimension 34)	Inverse variance weighted	36	0.01 (0.00 to 0.54)	0.0250
T1 brain MRIs UDIPs (dimension 39)	Inverse variance weighted	36	97.54 (8.50 to 1119.58)	0.0002
T1 brain MRIs UDIPs (dimension 49)	Inverse variance weighted	36	55.00 (2.55 to 1188.39)	0.0106
T1 brain MRIs UDIPs (dimension 96)	Inverse variance weighted	36	62.08 (1.05 to 3687.72)	0.0476
T1 brain MRIs UDIPs (dimension 38)	Inverse variance weighted	36	74.54 (2.48 to 2235.87)	0.0130
T1 brain MRIs UDIPs (dimension 39)	Inverse variance weighted	36	0.03 (0.00 to 0.93)	0.0452
T1 brain MRIs UDIPs (dimension 59)	Inverse variance weighted	36	10998.67 (9.00 to 13435644.00)	0.0103
T1 brain MRIs UDIPs (dimension 68)	Inverse variance weighted	36	233.91 (1.27 to 42989.78)	0.0403
T1 brain MRIs UDIPs (dimension 113)	Inverse variance weighted	36	2158.07 (6.98 to 666825.07)	0.0087
T1 brain MRIs UDIPs (dimension 126)	Inverse variance weighted	36	690.52 (1.75 to 272617.69)	0.0321
T2 brain MRIs UDIPs (dimension 30)	Inverse variance weighted	36	0.13 (0.02 to 0.71)	0.0185
T2 brain MRIs UDIPs (dimension 40)	Inverse variance weighted	36	11.12 (1.33 to 92.96)	0.0261
T2 brain MRIs UDIPs (dimension 70)	Inverse variance weighted	36	0.07 (0.01 to 0.88)	0.0392
T2 brain MRIs UDIPs (dimension 80)	Inverse variance weighted	36	84.84 (4.03 to 1788.13)	0.0043
T2 brain MRIs UDIPs (dimension 113)	Inverse variance weighted	36	0.04 (0.00 to 1.00)	0.0500
T2 brain MRIs UDIPs (dimension 123)	Inverse variance weighted	36	0.12 (0.02 to 0.83)	0.0310
T2 brain MRIs UDIPs (dimension 54)	Inverse variance weighted	36	0.01 (0.00 to 0.53)	0.0238
T2 brain MRIs UDIPs (dimension 76)	Inverse variance weighted	36	83.93 (1.43 to 4940.92)	0.0331

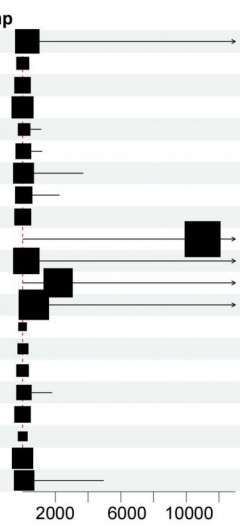

Exposure	Outcome	nsnp	HR (95% CI)	pval
C−C motif chemokine 23 levels	T1 brain MRIs UDIPs (dimension 14)	31	0.01 (0.00 to 0.10)	0.0000
C−C motif chemokine 23 levels	T2 brain MRIs UDIPs (dimension 96)	31	0.14 (0.03 to 0.78)	0.0244
C−X−C motif chemokine 11 levels	T2 brain MRIs UDIPs (dimension 13)	38	0.07 (0.01 to 0.78)	0.0309
Fibroblast growth factor 5 levels	T1 brain MRIs UDIPs (dimension 7)	29	43.38 (2.27 to 829.65)	0.0123
Fibroblast growth factor 5 levels	T2 brain MRIs UDIPs (dimension 15)	29	0.15 (0.02 to 0.88)	0.0354
Glial cell line−derived neurotrophic factor levels	T2 brain MRIs UDIPs (dimension 35)	25	0.03 (0.00 to 0.88)	0.0419
Osteoprotegerin levels	T1 brain MRIs UDIPs (dimension 46)	30	10409.26 (8.13 to 13334809.17)	0.0113
Osteoprotegerin levels	T2 brain MRIs UDIPs (dimension 96)	30	0.09 (0.01 to 0.86)	0.0368